Dyes and Pigments 207 (2022) 110746

Contents lists available at ScienceDirect

Dyes and Pigments

journal homepage: www.elsevier.com/locate/dyepig

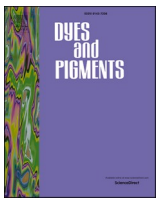

Synthesis and fluorescence of N-squaraine dianions derived from electron-deficient primary anilines

Manel Vega, Rosa M. Gomila, Jordi Pons, Antonio Frontera, Carmen Rotger, Antonio Costa *

Departament de Química, Facultat de Ciències, Universitat de les Illes Balears, Ctra. Valldemossa, Km 7.5, Palma, 07122, Spain

ARTICLE INFO

Keywords:
Squaraine dyes
Dianion
Fluorescence
DFT calculations

ABSTRACT

Squaraines are 1,3-disubstituted squaric acid derivatives featuring intense fluorescence in the visible. Unlike their parent compounds, N-squaraines obtained by condensation reaction between squaric acid and primary anilines are non-fluorescent compounds. The incorporation of electron-withdrawing substituents in the para position of the phenyl rings turns these compounds acidic enough to form the corresponding dianions by acid-base reaction with alkaline hydroxide in mixed DMSO-H_2O solvent mixtures. This work reports the microwave-assisted synthesis of N-squaraines and the investigation of the optical characteristics of their dianions. The dianionic squaraines have a $C_4N_2O_2^{2-}$ squaryl core with absorption maxima at 450–748 nm (molar absorptions up to 7.6×10^4 M^{-1} cm^{-1}). The N-squaraine dianions are highly fluorescent in the 507–644 nm range (quantum yields 0.18–0.72). Due to their negative charge, and contrary to the expectations, anionic N-squaraines are chemically stable for hours in 50% v/v H_2O–DMSO solvent mixtures. DFT calculations show the absorption bands are $S_0 \rightarrow S_1$ excitations (HOMO → LUMO) and $S_1 \rightarrow S_0$ transitions (LUMO → HOMO) for the emission. In both cases, the calculated wavelengths compare well with the experimental observations.

1. Introduction

Squaraines (SQs) are 1,3-disubstituted squaric acid derivatives featuring two electron-rich substituents flanking a squaryl ($C_4O_2^-$) deficient core (Chart 1). Since early applications in photoelectronic devices [1], many material science and biomedicine applications have entered the stage [2] Nowadays, SQs are critical components in multiple photoactive materials, including solar cells [3–5], active fluorescent reporters for ions [6], biological labelings [7,8] and bioimaging [9–11].

Based on their structural characteristics, there are two main types of SQs, namely arene- and arylidene-SQs. Both types are rigid planar compounds exhibiting intense and sharp absorption bands ($\varepsilon \approx 3 \times 10^5$ $M^{-1}cm^{-1}$), high fluorescent intensities in the visible [12–14], and excellent photostability compared to other cyanine-type compounds. Aniline-based squaraines are a subgroup of SQ compounds formed via regioselective condensation of electron-rich N,N-disubstituted anilines with squaric acid (Chart 1A). The reaction occurs through the *para* C_{Ar}-position of the phenyl ring and encompasses most arylamine squaraines already reported.

However, the condensation of squaric acid with primary and secondary alkyl- or aryl amines, including anilines [15,16], takes a different route. In this case, the reaction occurs through the nitrogen atom leading to symmetrically substituted squaraine compounds featuring the two nitrogen atoms directly bonded to the squaryl moiety. Hereafter, we named these compounds N-squaraines (NSQ) for distinction (Chart 1B).

Despite their almost parallel historical and common chemical origin, only a few studies investigate the properties of NSQs compared to the broad spectra of applications already reported for canonical SQs. Notable exceptions are the work by Kabatc et al. on NSQs as photoinitiators for photopolymerization reactions [17,18]. Also, a report by Wang et al. describes an NSQ-based colorimetric chemosensor for carbon dioxide. In this work, the sensing strategy is based on removing the two N–H protons of a nitro-derived NSQ, thus recognizing the critical role of the acid-base equilibria that characterize NSQ compounds [19].

One of the reasons for the lack of work on NSQs is their expected chemical degradation in front of nucleophiles due to the presence of the iminium group directly bonded to the electron-deficient squaryl ring. Hydrolytic degradation [20], and nucleophilic bleaching by thiols [21], cyanide anion [22] and phosphorus (III) derivatives [23] are known issues hampering the use of aniline-derived SQs. Nevertheless, the development of protected arene-squaraine has proven helpful for overcoming these limitations in biological labeling [24]. The low intrinsic

* Corresponding author.
E-mail address: antoni.costa@uib.es (A. Costa).

https://doi.org/10.1016/j.dyepig.2022.110746
Received 30 May 2022; Received in revised form 29 July 2022; Accepted 11 September 2022
Available online 17 September 2022

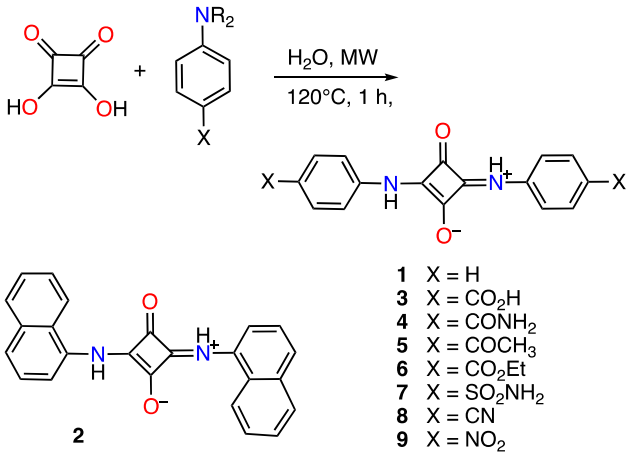

Scheme 1. Microwave-Assisted Synthesis of Symmetrical N-squaraines **1**–**9**.

fluorescence intensity of NSQs ($\Phi_f < 0.025$) compared to SQs is a second negative aspect that reduces their potential applications [25,26]. However, and in this line, we recently reported a bis-cyano N-squaraine **8** (X = CN) that produced a highly fluorescent silver dianionic complex by the combined action of Ag(I) and acetate as the base [27].

Apart from the Lewis acid character of Ag(I) and its role in promoting the deprotonation of the N-squaraines, we became interested in the high fluorescence response of the bis-cyano N-squaraine dianion. This observation is especially relevant considering the low or null fluorescence intensities observed for this squaraine in its protonated forms. In standard anilino squaraines (SQ-type), the electron-donating substituents of the aryl rings decrease the HOMO-LUMO gap and increase the D-A-D character of the long-wavelength absorbing band responsible for their fluorescent response [13,28]. However, NSQs present substantial structural differences compared to SQs. Upon deprotonation, the original π-system of NSQs evolves to two linear conjugated systems that can be represented by a set of degenerated resonance structures or, more simply, by the ideal form with partial bonds represented in Chart 2. This structure is more likely viewed as an A-π-A-π-A system, distinct from the classical D-π-A-π-D pattern found in related electron-donating SQs. We envisaged that this rather unusual conjugated π-system could account for the fluorescent response of NSQs. To support our hypothesis, a very recent report by Shandura et al. describes a set of highly fluorescent dianionic dioxaborines, structurally different from NSQs, but featuring an A-π-A-π-A conjugated system related to that studied here [29].

In this work, we report the synthesis and characterization of dianionic N-squaraines **1**–**9** (Chart 2) composed of a central squaraine core and two aniline aryl rings decorated with electron-withdrawing groups (EWG) in para position. Using a combined experimental and theoretical approach, we demonstrate that these NSQs form intrinsically fluorogenic dianions in alkaline DMSO either alone or in mixtures with water.

2. Experimental

2.1. Material synthesis and characterization

All chemicals were obtained from commercial sources and used without further purification unless otherwise indicated. All reactions were performed in a single-mode Biotage Initiator microwave reactor according to the parameters described below. Proton nuclear magnetic resonance (^{1}H NMR) spectra and carbon nuclear resonance (^{13}C NMR) were recorded at room temperature on a Bruker Avance and Bruker Avance III spectrometers operating at 300 and 600 MHz for ^{1}H and 75.4 and 150.9 MHz for 13-carbon, respectively. The residual proton signal in the NMR solvent was used as a reference (DMSO-d_6: δ 2.50 ppm). Chemical shifts (δ) are reported in ppm and coupling constants (J) in Hz. Multiplicities for proton signals are abbreviated as s, t, m, and br for singlet, triplet, multiplet, and broad signal, respectively. ^{13}C-*CP-MAS NMR* spectra, including spinning sidebands, were obtained on a Bruker SB-MAS probe head with 4 mm ZrO_2 MAS rotors, spinning rate 10 kHz, and externally referenced to adamantane at 38.5 ppm. High-resolution mass spectra (HRMS) were recorded on a Thermo Scientific Orbitrap Q-Exactive mass spectrometer equipped with a heated electrospray module (HESI-HRMS) or on a Bruker Autoflex III MALDI–TOF, using a CHCA or DCTB matrix, and PEG300 or PEG400 for calibration. FT-IR spectra were obtained on Bruker FT-IR Tensor 27 on KBr pellets. Spectral features are tabulated as follows: wavenumber (cm^{-1}); intensity: strong (s), medium (m), and weak (w).

2.1.1. General synthetic procedure for preparation of N-squaraines

A mixture of squaric acid (58 mg, 0.5 mmol) and a slight excess of the corresponding 4-substituted aniline (1.2 mmol) suspended in water (1.5 mL) was heated at 120 °C with stirring under microwave irradiation (25 w) for 1h (Scheme 1). Then the solid N-squaraine was filtered under vacuum and washed sequentially with 1 N HCl (3 × 10 mL), 10% (v/v) DMSO-ethyl acetate (5 × 10 mL), and ethyl acetate (3 × 10 mL) unless otherwise stated. The remaining solid was air-dried and then oven-dried at 105 °C for 3h.

2.1.2. Synthesis of N-squaraine 1 (R = H) [16,30,31]

The title compound was obtained as a yellow solid; yield 43 mg (33%); mp > 300 °C. ^{1}H NMR (DMSO-d_6) δ_H 11.42 (s, 2H, –NH–), 7.79 (br, 4H, -Ar), 7.38 (br, 4H, -Ar), 7.13 (br, 2H, -Ar) ppm. ^{13}C CP-MAS NMR: δ_C 173.7 (C═O), 169.2 (C–N), 138.1 (-Ar), 130.2 (-Ar), 124.1 (-Ar), 122.3 (-Ar) ppm. IR (KBr; cm^{-1}): 3179, 3128, 3088, 2993, 2967, 2937 (=C–H); 1590 (C–O), 1552 (N–H); 1450, 1426 (C–C); 1338, 1245 (C–N); 825,794,750, 688 (C–H).

2.1.3. Synthesis of N-squaraine 2 (R = Napth) [16]

This compound was obtained through a modification of the general procedure. A mixture of squaric acid (58 mg, 0.5 mmol) and 1-naphthylamine (172 mg, 1.2 mmol) suspended in water (2 mL) was heated with stirring in a closed vial at 150 °C for 12 h in a sand bath. The resulting

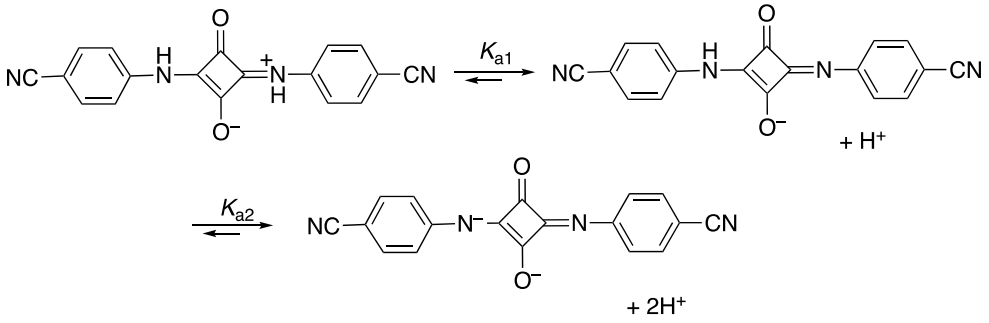

Scheme 2. Acid-base equilibria operating in NSQ **8**.

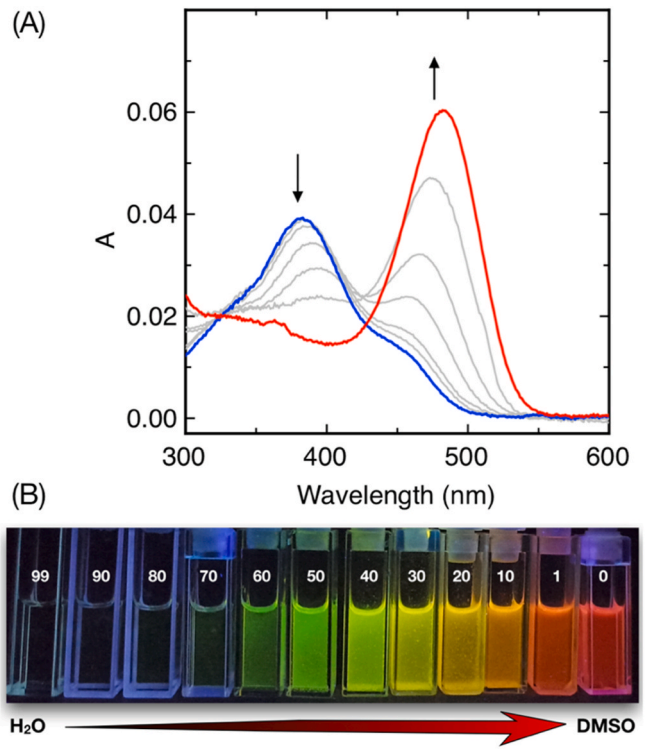

Fig. 1. (A) Absorption spectra of NSQ **8** (1.0×10^{-6} M) dissolved in different DMSO-H_2O (0.1 M NaOH) mixtures: (1:99), (5:95), (10:90), (20:80), (30:70), (40:60), and (50:50) v/v, respectively. (B) Fluorescence image recorded with a 365 nm handheld lamp of NSQ **8** (2.0×10^{-6} M) dissolved in different DMSO-H_2O (1.0 M NaOH) mixtures, the percentage of water in volume is indicated within the image. The dianion in 100% DMSO was generated using tetramethylammonium hydroxide (0.025 M) as the base.

solid was filtrated in vacuum, washed with methylene chloride until the extracts went clear, then with hot ethyl acetate (5 × 10 mL) and ethanol (5 × 10 mL). The remaining solid was dried as usual. The title compound was obtained as a brown solid; yield 164 mg (92%); mp > 300 °C. ^{1}H NMR (300 MHz, DMSO-d_6): δ_H 11.66 (s, 2H, –NH–), 8.17 (d, J = 7.2 Hz, 2H, -Ar), 7.98 (d, J = 7.5 Hz, 2H, -Ar), 7.84 (t, J = 4.2 Hz, 2H, -Ar), 7.6–7.54 (br, 8H, -Ar) ppm. ^{13}C CP-MAS NMR δ_C 175.9 (C–O), 170.4 (C–N), 132.5 (Ar), 125.8 (Ar), 121.1 (Ar) ppm. IR (KBr; cm^{-1}): 3154, 3122, 3071, 2995, 2957 (=C–H); 1598 (C–O); 1552, 1506 (N–H); 1395, 1368 (C–C); 1272, 1254 (C–N); 795, 767 (C–H). ESI(−)-HRMS *m/z* (%) calcd for $C_{24}H_{15}N_2O_2$: $[M - H]^-$ 363.11280; found 363.11342.

2.1.4. Synthesis of N-squaraine **3** ($R = CO_2H$) [32]

After microwave heating and filtration, the title compound was washed with water. Then, the resulting solid was removed and digested three times with 5% solution of $NaHCO_3$ (50 mL) for 2 h. The solid was isolated by centrifugation (4000 rpm, 10 min), washed with 1 N HCl (3 × 20 mL) and water (3 × 20 mL), and dried to afford the title compound as a yellow solid, yielding 135 mg (78%); mp > 300 °C. ^{1}H NMR (300 MHz, DMSO-d_6): δ_H 12.85 (s, 2H, –COOH), 11.83 (s, 2H,–NH–), 7.91 (m, 8H, -Ar) ppm. ^{13}C CP-MAS NMR δ_C 174.1 (C–O), 171.1 (COOH), 169.3 (C–N), 140.2 (-Ar), 131.8 (-Ar), 127.2 (-Ar), 119.7 (-Ar), 118.0 (-Ar) ppm. IR (KBr; cm^{-1}): 3073, 2990 (=C–H); 1687 (C═O); 1604 (C–O); 1556, 1517 (N–H); 1419 (C–C); 1282 (C–O); 1248,1195 (C–N); 856, 840, 804, 771 (C–H). ESI(−)–HRMS *m/z* (%) calcd for $C_{18}H_{11}N_2O_6$: $[M - H]^-$ 351.06226; found 351.06237.

2.1.5. Synthesis of N-squaraine **4** ($R = CONH_2$)

After microwave heating and filtration, the solid was taken in 5% HCl (10 mL), filtered again and washed with 5% HCl (3 × 10 mL), 30% (v/v) of DMSO – EtOAc (3 × 10 mL), EtOAc (3 × 10 mL) and dried. The title compound was a yellow solid, yield 160 mg (91%); mp > 300 °C. ^{1}H NMR (300 MHz, DMSO-d_6): δ_H 11.73 (s, 2H, –NH–), 7.88 (bs, 10H, -Ar), 7.35 (s, 2H, -Ar) ppm. ^{13}C CP-MAS NMR δ_C 173.9 (C–O), 169.7 (C–N), 139.2 (-Ar), 130.3 (-Ar), 127.5 (-Ar), 118.3 (-Ar) ppm. IR (KBr; cm^{-1}): 3406, 3187 (N–H); 3070, 2989 (C–H); 1662 (C═O); 1605 (C–O); 1553 (N–H); 1414 (C–C); 1255, 1205 (C–N); 849, 835, 802, 772 (C–H). MALDI-TOF-HRMS *m/z* (%) calcd for $C_{18}H_{15}N_4O_4$: $[M+H]^+$ 351.1090; found 351.1088.

2.1.6. Synthesis of N-squaraine **5** ($R = COCH_3$)

The title compound was obtained as a yellow solid, yielding 168 mg (96%) from 4-aminoacetophenone, and 145 mg (90%) from 4-ethynylaniline. With 4-ethynylaniline a complete Markovnikov-type alkyne hydration promoted by the squaric acid takes place in the aqueous medium

Table 1
pK_a values[a] in 50:50 v/v DMSO-water, I = 0.1 M (KCl), at 298.1 ± 0.1 K

NSQ	X	σ_p	pK_{a1}	pK_{a2}
3	CO_2H	0.40	13.3(2)	15.3(2)
5	$COCH_3$	0.45	12.7(2)	13.0(5)
8	CN	0.66	12.1(6)	13.5(5)
9	NO_2	0.78	10.3(5)	12.5(4)

[a] Measured in in 50:50 v/v DMSO-water, I = 0.1 M (KCl), at 298.1 ± 0.1 K. Values in parenthesis are standard deviations in the last significant figures.

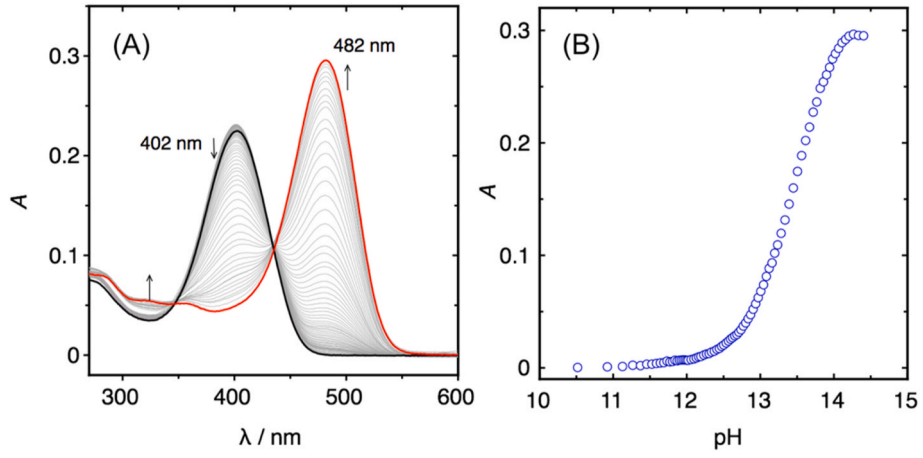

Fig. 2. (A) Consecutive absorption spectra of a (50:50 v/v) DMSO-H_2O solution of **8** (1.0×10^{-5} M, $pH_{init} \approx 10$) in the range 260–600 nm. The arrows indicate the change in absorbance upon titration with a base (OH^-) (B) pH dependence of the band intensity at 482 nm.

Table 2
Spectroscopic characteristics of NSQs **1**–**9** in (99:1 v/v DMSO-H_2O, 0.1 N NaOH).

NSQ	X	λ_{abs} [a] (nm)	$\varepsilon \times 10^{-4}$ ($M^{-1}cm^{-1}$)	λ_{exc} (nm)	λ_{em} (nm)	Φ_f	$\Delta\lambda$ [b] (nm)	$\Delta\lambda$ [b] (cm^{-1})
1	H	459	7.1(1)	459	510	0.0(4)	51	2179
2	Napth.	539	4.3(6)	539	609	_[c]	70	2133
3	COO^-	487	4.0(9)	487	526	0.3(4)	39	1522
4	$CONH_2$	527	7.7(4)	526	574	0.3(6)	47	1554
5	$COCH_3$	593	7.1(9)	595	644	_[c]	51	1335
6	CO_2Et	554	7.6(9)	553	599	0.2(2)	45	1356
7	SO_2NH_2	480	6.5(2)	478	507	0.2(6)	27	1109
8	CN	545	8.6(6)	545	587	0.7(2)	42	1313
9	NO_2	748	4.8(1)	_[d]	_[d]	_	_	_

[a] Wavelength maxima assuming the complete conversion to the dianionic form.
[b] Stokes shift.
[c] Not determined due to chemical degradation.
[d] Non-fluorescent.

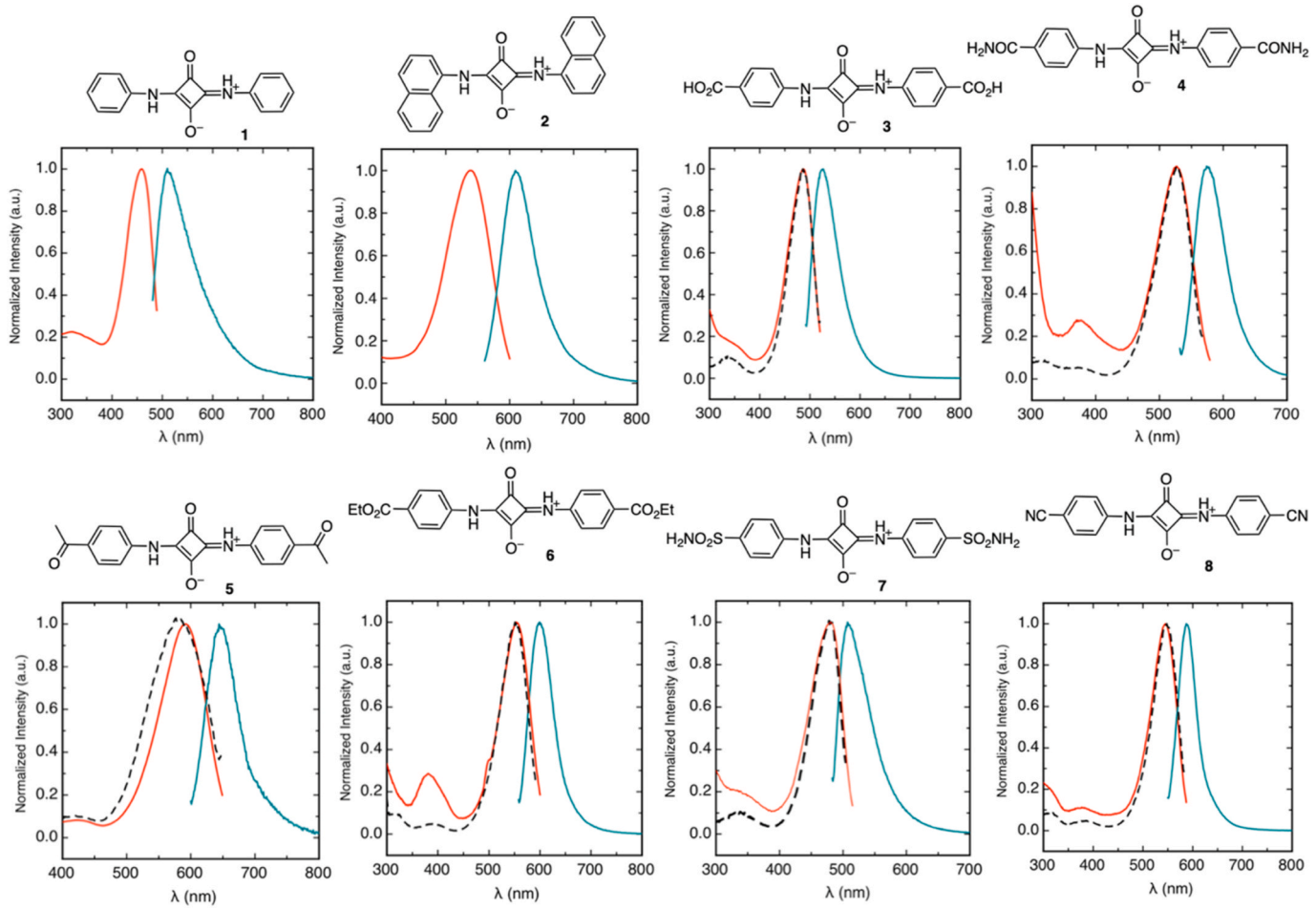

Fig. 3. Normalized UV–vis absorption (red), emission (green), and excitation spectra (discontinued line, not recorded for **1** and **2**) of NSQs **1**–**8** dianions in 99:1 v/v DMSO-H_2O, 0.1 N NaOH.

[33]. mp > 300 °C. ^{1}H NMR (600 MHz, DMSO-d_6): δ_H 11.90 (s, 2H, –NH–), 8.02 (d, J = 8.4 Hz, 4H, -Ar), 7.94 (br, 4H, -Ar), 2.56 (s, 6H, CH_3) ppm. ^{13}C CP-MAS NMR δ_C 197.3 (C═O), 173.8 (C–O), 169.2 (C–N), 139.9 (-Ar), 134.4 (-Ar), 132.7 (-Ar), 130.3 (-Ar), 128.8 (-Ar), 120.4 (-Ar), 119.1 (-Ar), 25.4 (CH_3) ppm. IR (KBr; cm^{-1}):3172, 3118, 3061, 2962 (=C–H); 1678 (C═O), 1598 (C–O); 1548 (N–H); 1415 (C–C); 1271 (C–N); 1192 (C–C); 835, 763, 694 (C–H). ESI(−)–HRMS *m/z* (%) calcd for $C_{20}H_{15}N_2O_4$: $[M-H]^-$ 347.10373; found 347.10399.

2.1.7. Synthesis of N-squaraine **6** ($R = CO_2Et$) [34]

The title compound was a yellow solid, yield 173 mg (85%) mp > 300 °C. ^{1}H NMR (600 MHz, DMSO-d_6): δ_H 11.90 (s, 2H, –NH–), 7.95 (br, 8H, -Ar), 7.94 (br, 4H, -Ar), 4.30 (q, J = 7.2 Hz, 4H, –CH_2-), 1.32 (t, J = 7.2 Hz, 6H, –CH_3) ppm. ^{13}C CP-MAS NMR δ_C 174.5 (C–O), 169.5 (C═O), 163.7 (C–N), 140.0 (-Ar), 131.8 (-Ar), 130.9 (-Ar), 127.7 (-Ar), 120.0 (-Ar), 60.3 (–CH_2–), 15.0 (-CH_3) ppm. IR (KBr; cm^{-1}): 3239, 3179, 3123, 3068, 2980 (=C–H); 1715 (C═O); 1585 (C–O); 1553 (N–H); 1420 (C–C); 1278 (C–N); 1188, 1109 (C–C(O)–C); 855, 768 (C–H). MALDI-TOF-HRMS *m/z* (%) calcd for $C_{22}H_{21}N_2O_6$: $[M+H]^+$ 409.1375; found

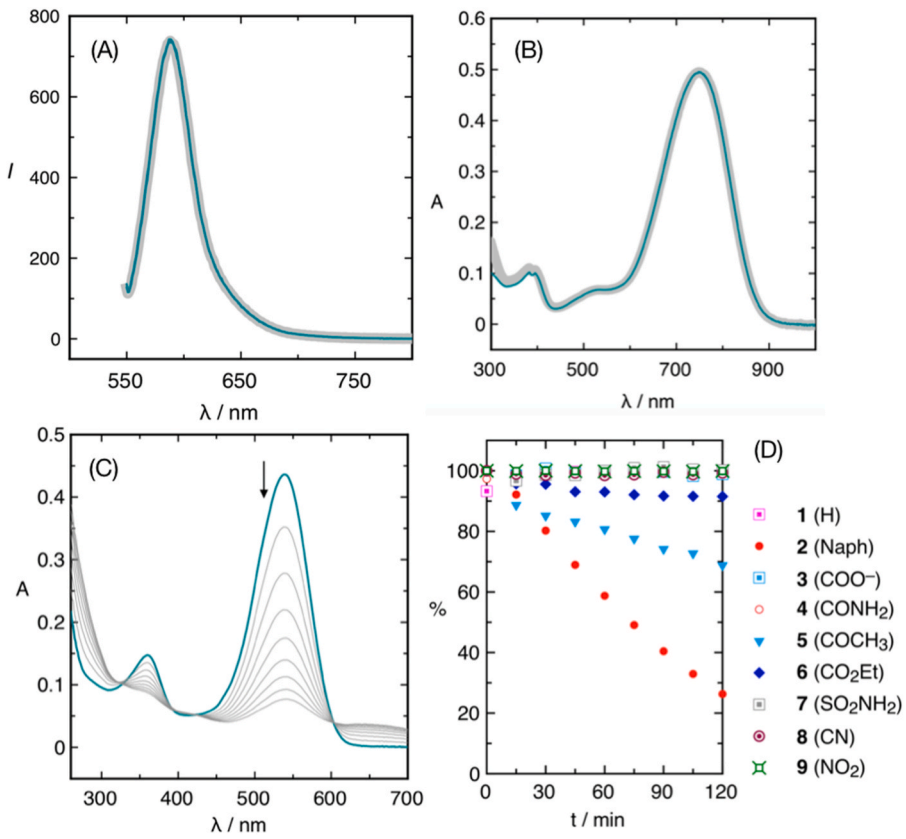

Fig. 4. (A) Superposition of NSQ **8** (2.0×10^{-7} M; $\lambda_{exc.} = 545$ nm) fluorescence emission spectra in 99:1 v/v DMSO-H_2O (0.1 N NaOH) recorded at 15 min time intervals from t = 0 (turquoise line) to t = 120 min (broad grey line). (B) Superposition of NSQ **9** (1.0×10^{-5} M) UV–vis spectra recorded as described in (A). (C) Superposition of NSQ **2** (1.0×10^{-5} M) UV–vis spectra recorded in 99:1 v/v DMSO-H_2O (0.1 N NaOH) at 15 min time intervals from t = 0 (turquoise line). (D) Comparative degradation of NSQs **1**–**9** over time.

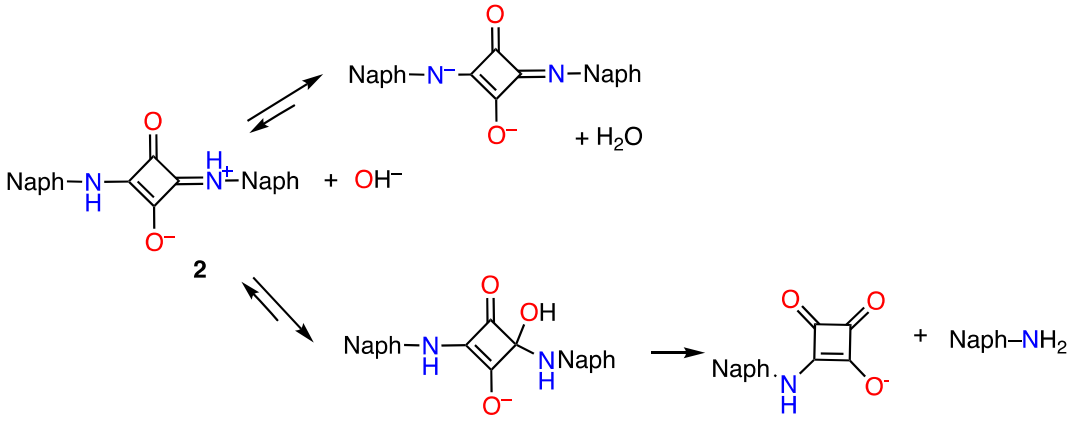

Scheme 3. Proposed chemical degradation route of N-squaraine **2** in alkaline media.

409.1394.

*2.1.8. Synthesis of N-squaraine **7** (R = SO_2NH_2)*

After microwave heating and filtration, the solid was taken in water and refluxed for 5 min, and filtered. This treatment was repeated three times. The title compound was a yellow solid, yield 190 mg (90%); mp > 300 °C. ^{1}H NMR (300 MHz, DMSO-d_6): δ_H 11.89 (s, 2H, –NH–), 7.91 (d, J = 8.4 Hz, 4H, -Ar), 7.81 (d, J = 8.7 Hz, 4H, -Ar), 7.35 (s, 4H, SO_2NH_2) ppm. ^{13}C CP-MAS NMR δ_C 174.4 (C–O), 168.9 (C–N), 140.4 (-Ar), 139.6 (-Ar), 132.3 (-Ar), 130.1 (-Ar), 128.2 (-Ar), 118.8 (-Ar) ppm. IR (KBr; cm^{-1}): 3347, 3261 (N–H); 3121, 3064, 2975 (=C–H); 1588 (C–O); 1548 (N–H); 1424, 1413 (C–C); 1341 (S=O); 1249 (C–N); 1162 (S=O); 850, 726 (C–H). ESI(−)–HRMS *m/z* (%) calcd for $C_{16}H_{13}N_4O_6S_2(S^{32})$ $[M - H]^-$ 421.02820; found 421.02791.

*2.1.9. Synthesis of N-squaraine **8** (R = CN)*

Was obtained as described in the general procedure, and it has recently been described by us [27].

*2.1.10. Synthesis of N-squaraine **9** (R = NO_2) [31]*

The title compound was a yellow-orange solid, yield 159 mg (90%); mp > 300 °C. ^{1}H NMR (300 MHz, DMSO-d_6): δ_H 12.25 (s, 2H, –NH–), 8.29 (d, J = 8.7 Hz, 4H, -Ar), 8.03 (br, 4H, -Ar) ppm. ^{13}C CP-MAS NMR δ_C 174.0 (C–O), 168.6 (C–N), 147.0 (-Ar), 142.1 (-Ar), 126.4 (-Ar), 120.81 (-Ar) ppm. IR (KBr; cm^{-1}): 3198, 3155, 3075, 2990 (=C–H); 1586 (NO_2); 1559 (C–O); 1512 (N–H); 1405 (C–C); 1339, 1311 (NO_2); 1251 (C–N); 861, 847 (C–H). MALDI-TOF-HRMS *m/z* (%) calcd for $C_{16}H_{11}N_4O_6$: $[M+H]^+$ 355.06786; found 355.06683.

Table 3
TDDFT calculations at the B3LYP/def2-TZVP level and experimentally obtained absorption maximum.

Comp.	X	excitation	λ_{calc} [a] (nm)	Main orbital transition	f	λ_{abs} [b] (nm)
1	H	$S_0 \rightarrow S_1$	420	HOMO→LUMO (99.9%)	1.66	459
2	Napth	$S_0 \rightarrow S_1$	583	HOMO→LUMO (90.2%)	1.31	539
3	COO^-	$S_0 \rightarrow S_1$	413	HOMO→LUMO (98.9%)	2.17	487
4	$CONH_2$	$S_0 \rightarrow S_1$	490	HOMO→LUMO (100%)	2.29	527
5	$COCH_3$	$S_0 \rightarrow S_1$	571	HOMO→LUMO (100%)	2.38	593
6	CO_2Et	$S_0 \rightarrow S_1$	484	HOMO→LUMO (100%)	2.46	554
7	SO_2NH_2	$S_0 \rightarrow S_1$	443	HOMO→LUMO (100%)	2.52	480
8	CN	$S_0 \rightarrow S_1$	507	HOMO→LUMO (100%)	2.39	545

[a] Calculated absorption maximum in DMSO.
[b] Observed absorption maximum in DMSO.

2.2. pKa determinations

The acidic thermodynamic constants were determined by spectrophotometric titrations in 50% (v/v) DMSO-water mixtures (0.1 M KCl, ionic strength) at recording the spèctra between 260 and 600 nm. Temperature control at 25 ± 0.1 °C was attained by circulating water with a Peltier thermostated accessory. Titrations were performed against pH starting at pH = 9 and adding increasing amounts of a standardized solution of NaOH (0.1–0.5 M) in the same solvent mixture. Data sets were analyzed with HypSpec14 (Protonic Software). In 50% v/v DMSO-H_2O (20% DMSO: 80% H_2O M) at 25 °C the activity of water is 0.447 (-log a_w = 0 0.349) [35] very different to the ideal value of 1 used as standard in pure water. In this medium the pK_w value is 15.5 [36,37].

2.3. Optical properties

UV/Vis absorption spectra were recorded on Cary 60 or Cary 300 UV–Vis–NIR equipped with a Peltier thermostated cell holder device temperature-control unit (ΔT ± 0.05 °C). Fluorescence excitation-emission spectra were recorded on a Cary Eclypse spectrophotometer at 25 ± 1 °C in 1 cm quartz glass cuvettes using spectroscopic grade solvents. Slit widths were set to 5 mm bandpass for both excitation and emission. Solutions of N-squaraines were prepared in DMSO or DMSO–H_2O mixtures of variable composition, as indicated in the text. The solutions were allowed to stand for 5 min before obtaining absorption and emission spectra. Quantum yields (Φ) were obtained by comparison of the integrated area of the emission spectrum of the sample under study relative to fluorescein ($\Phi_{ref.}$ = 0.91, NaOH 0.1 N), Rhodamine 6G ($\Phi_{ref.}$ = 0.91, EtOH), Rhodamine 101 ($\Phi_{ref.}$ = 0.915, EtOH) or Coumarin 153 ($\Phi_{ref.}$ = 0.53, EtOH). Refractive indexes: 1.476 for DMSO, 1.359 for EtOH and 1.33 for water. Fluorescence intensities were obtained by integrating the emission spectra over their full spectral range. All measurements were made in triplicate and averaged.

2.4. Computational methods

All calculations were performed using the ORCA [38] software package (ORCA-ESD module). All structures were optimized using the B3LYP functional [39–41] and the def2-TZVP [42] basis set. For the computation of two-electron integrals, the resolution of identity approximation was used for the Coulomb part (RIJ) with the corresponding auxiliary basis. For the excited states, TDDFT with the Tamm-Dancoff approximation was employed [43]. It has been

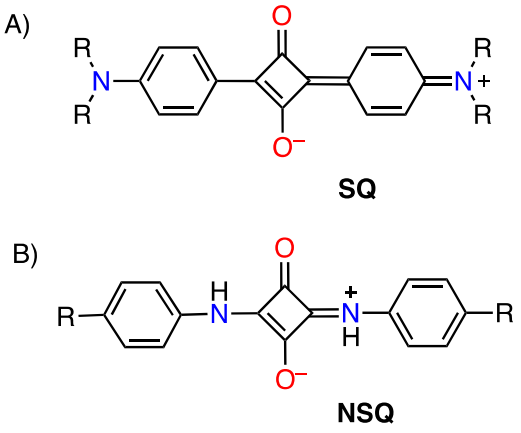

Chart 1. Representative mesoionic structures of the two possible aniline-derived squaraines. A) C_{Ar} -SQ bonded, and B) N,N-SQ bonded, referred to as SQ and NSQ, respectively.

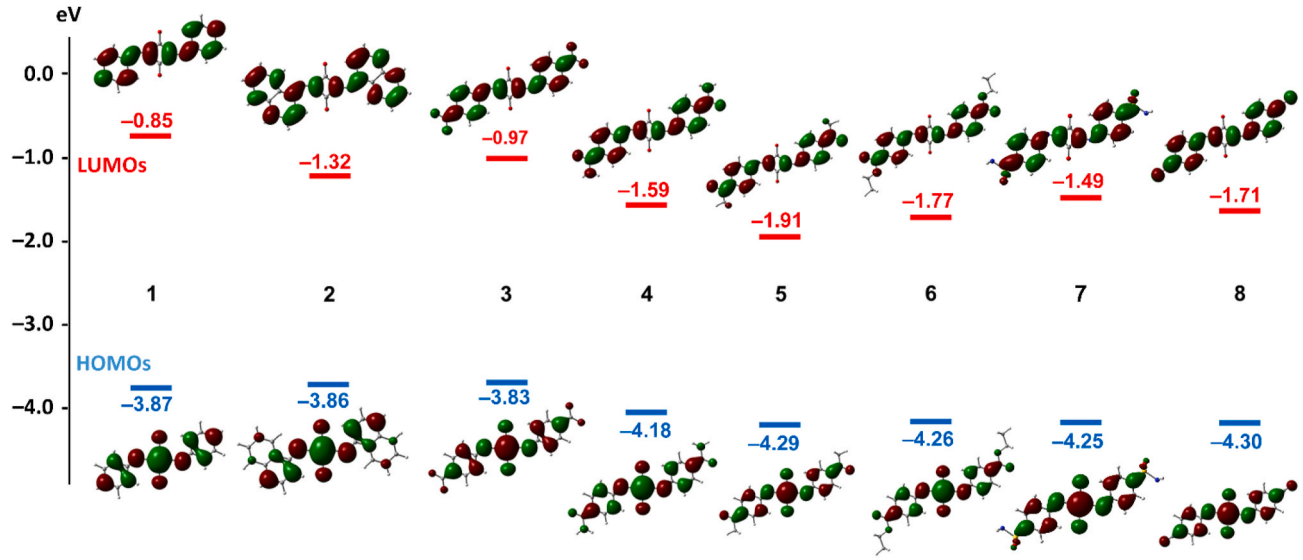

Fig. 5. Molecular orbital energy diagrams and isodensity surface plots of HOMOs and LUMOs of NSQs **1**–**8**.

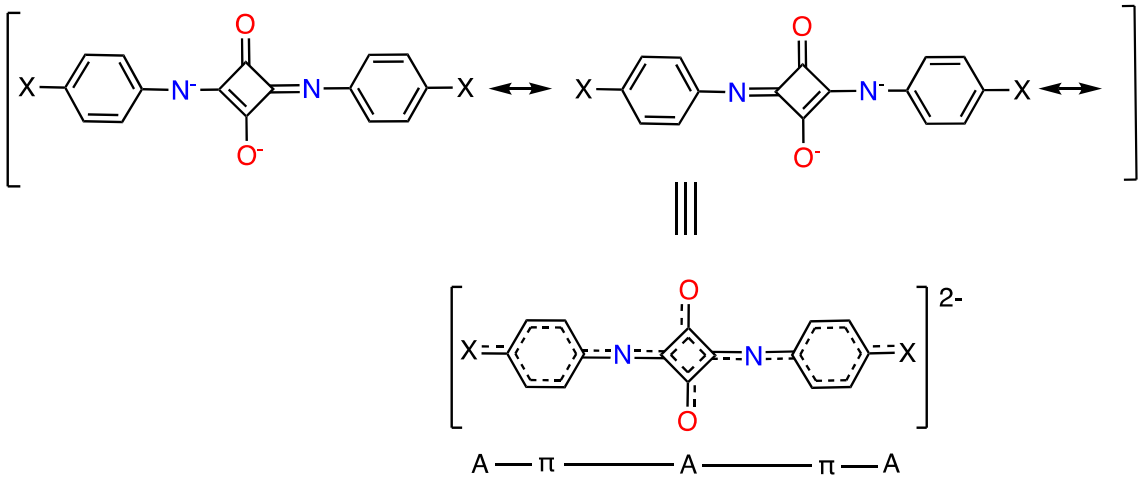

Chart 2. Some resonance structures of NSQs dyes investigated herein.

Table 4
Photophysical parameters calculated from the path integral approach at the B3LYP/def2-TZVP level of theory.

Comp.	X	emission	λ_{calc} [a] (nm)	k_f (s^{-1})	λ_{exp} [b] (nm)
1	H	S0 ← S1	457	9.3×10^8	510
2	Napth	S0 ← S1	595	4.1×10^8	609
3	COO^-	S0 ← S1	481	1.1×10^9	526
4	$CONH_2$	S0 ← S1	555	7.9×10^8	574
5	$COCH_3$	S0 ← S1	643	5.7×10^8	644
6	CO_2Et	S0 ← S1	592	7.1×10^8	599
7	SO_2NH_2	S0 ← S1	560	7.4×10^8	507
8	CN	S0 ← S1	571	7.6×10^8	587

[a] Calculated and experimental emission maxima in DMSO.
[b] Calculated and experimental emission maxima in DMSO.

demonstrated that this approximation to TDDFT reduces the computational cost for the B3LYP functional and yields excited state transition energies, which are typically of the same quality as those which are obtained from TDDFT itself [44]. We searched for the first 10 roots and used the one that represents the first excited state from the experiment. This is reasonable since, in all cases, the lowest lying transition corresponds to S0→S1 transitions (vide infra). Moreover, to further support this criterion, in one compound (NSQ **8**), we have used 20 roots, obtaining identical results. The convergence criteria for both the SCF and geometry optimizations were set to TIGHT. The DFT grid was set to GRID4, and all the other parameters were chosen as default. The optimization of the geometries and the calculations of the fluorescence rate constants (obtained from the transition dipoles) were done in DMSO after the application of the linear response conductor-like polarizable continuum model (LR-CPCM) perturbation of the density. The theoretical prediction of fluorescence rates and absorption and emission spectra from first principles was made using the path integral approach [45].

3. Results and discussion

Classical syntheses of symmetrical NSQs involve condensing squaric acid with 2 M excess of the aniline in DMF or DMSO [16] or refluxing the mixture of both compounds in *n*-BuOH/toluene solvent mixtures with azeotropic removal of water [46]. In this work, we set up a greener and chemoselective approach using water as the solvent and performing the condensation under microwave heating at 120 °C for 1 h. Using this procedure, N-squaraines **1**–**9** were isolated in good yields (80–90%), and essentially free of contamination by the corresponding squaramides. Although the classical method of syntheses is also applicable here, we found our method more convenient in yield and selectivity towards N-squaraines (see Scheme 1)

N-squaraines derived from primary anilines are insoluble compounds in most ordinary solvents. They are weakly soluble in DMF and DMSO used for recording the ^{1}H NMR spectra but inadequate for recording the N-squaraines ^{13}C{H}NMR spectra in solution.

The simplicity of the ^{1}H NMR spectra indicates the symmetric C_2 arrangement of the two aryl rings around the central squaryl core. We used ^{13}C CP-MAS NMR spectroscopy to further characterize N-squaraines **1** to **9**. In all these cases, the spectra are reasonably simple, showing two characteristic well-resolved peaks at 174.0 ± 0.5 and 169.5 ± 1.0 ppm, respectively, that can be safely assigned to the two magnetically distinct squaryl carbons common to all NSQs.

3.1. NSQs acid-base properties and pK_a calculations

N-squaraines are ionizable compounds that, in a solution, can exist in three prototropic forms, neutral, monoanion, and dianion (Scheme 2). To prove the direct implication of the dianionic forms in the observed fluorescence, we evaluated the ionization constants of NSQs in DMSO-H_2O mixtures because of the lack of solubility of NSQs in pure water.

The UV–vis spectrum of NSQ **8**, taken as an example, in a basic aqueous solution (0.1 N, NaOH) containing 1% v/v of DMSO, shows a band at 380 nm corresponding to a mixture of the neutral and monoanionic forms. In contrast, the dianion band is hardly detected as a shoulder at around 460 nm (Fig. 1A). Upon increasing the percentage of DMSO, the dianionic band is visible at about 482 nm and becomes the only band observable in DMSO-water mixtures 50:50 v/v. The double ionization of the NSQs runs parallel to the high basicity of the hydroxide anion in DMSO (pKa 31.4) compared to water (pKa 15.75) [47]. The changes in the composition of the solvent mixture produced a bathochromic shift (c.a. 16 nm) of the two bands indicating negative solvatochromism, which is the expected behavior for anionic chromophores whose ground state is more polar than the excited state [48]. In fact, the DFT calculations reported herein show that the charges at the heteroatoms of the squaraine core are greater in the ground state than in the excited state. For instance, in compound **6**, the atomic charges at the N and O atoms at the ground state are – 0.23 and – 0.45 e, respectively, and they become smaller in absolute value in the excited state (– 0.19 and – 0.42 e for N and O-atoms, respectively). Here, the formation of NSQ dianions is likely crucial and directly related to the observed fluorescence of the NSQs (Fig. 1B).

The protonation constants of N-squaraines in (50:50 v/v) DMSO-H_2O mixtures were assessed by UV–vis spectrophotometric titrations. The mixed DMSO-H_2O medium provides an extensive acidity range (pK_w = 15.5), thus permitting the evaluation of deprotonation equilibria of weak acids that could hardly be studied in water [37]. However, N-squaraines **1** (X = H) and **2** (Naphtyl), lacking any

electron-withdrawing group (EWG), are weaker acidic compounds. Consequently, the absorption bands of their dianionic forms are only partially formed in 1:1 v/v DMSO-H_2O mixtures. On the other hand, NSQs **4** and **7** feature additional NH protons susceptible to ionization hampering data interpretation. Therefore, we used the UV–vis spectra of N-squaraines **3** (CO_2H), **5** ($COCH_3$), **8** (CN), and **9** (NO_2), which show similar trend patterns, and assuming they are diprotic acids, to obtain the corresponding pK_a values. Fig. 2A shows the UV–vis spectral differences due to changes in pH of a fixed (50:50 v/v) DMSO-H_2O solvent mixture of NSQ **8**. Upon titration with an alkaline base (OH^-), the initial band (402 nm; $\varepsilon \approx 10^4$ $M^{-1}cm^{-1}$; pH ≈ 10) exhibited a slight intensity increase but rapidly decreased upon further additions. Simultaneously, a new intense band appeared at 482 nm. The intensity of this band, assigned to NSQ **8** dianion, shows a sigmoid curve indicating the existence of an acid-base equilibrium (Fig. 2B), and the whole data were analyzed with HypSpec software to give the ionization constants depicted in Table 1 (see also, Fig. S18) [49]. Remarkably, the calculated acidity constants align with the Hammett substituent parameters (σ_p) reported for electron-withdrawing substituents [50]. Although too preliminary for deriving a complete explanation, these results suggest that the EWG substituents could increase the stability of the conjugated base of the "acidic" NH squaraine protons helping to delocalize the negative charge developed on the nitrogen atoms of the N-squaraines.

3.2. Photophysical properties of NSQs

Next, we move to DMSO-H_2O mixtures containing (99:1 v/v) of a 0.1 N NaOH solution. In this media, the hydroxide anion (pK_a ≈ 31) is stronger enough to deprotonate NSQs **1**–**9**, and NSQs become soluble due to their complete deprotonation. The observed absorption maxima range from 459 to 748 nm depending on the electron withdrawing character of the aryl substituent that participated in each chromophore. In all these cases, the long wavelength-absorbing band of the dianion is more intense than that of the protonated forms. For example, the molar extinction (ε) for NSQ **8** dianion is 86.000, *vs.* 62.000 $M^{-1}cm^{-1}$ for its corresponding mono- and di-protonated forms.

The fluorescence excitation and emission spectra of NSQs **1**–**9** (Table 2 and Fig. 3) were studied in the same solvent mixture by excitation close to the maxima of the respective dianion absorbing band. Pleasantly, NSQs **1**–**8** showed an emission band that, in all cases, was the mirror image of the lowest energy absorption band. Also, the excitation spectra recorded at the emission maxima matched the absorption spectra in every case, thus informing that the absorption band of the N-squaraine dianion and no other bands at shorter wavelengths were responsible for the observed fluorescence. The excitation at shorter wavelengths revealed no additional emission bands. The Stokes shifts ($\Delta\lambda$) range from 27 to 70 nm (1100–2180 cm^{-1}). These are moderate values indicative of a change in dipole moments between the ground and excited states of the previously formed dianion.

Despite having highly acidic NH hydrogen atoms (Table 1), and the longest wavelength dianionic absorption band among all the studied NSQs, N-squaraine **9** (X = NO_2) was non-fluorescent in all conditions already tested. Although the precise mechanism underlying the lack of fluorescence is unknown, the nitro group is commonly recognized as a fluorescence quencher group. The relatively high energy of the lone-pair electrons and the strong EWG effect of the NO_2 group provide effective ways for a radiationless deactivation of the chromophore in the excited state [51]. The fluorescence quantum yield of NSQ **8** dianion (X = CN; $\Phi_f = 0.72$ is remarkable since the value measured for **8** in its protonated neutral form in DMSO is negligible ($\Phi_f < 10^{-3}$). A similar trend, though less significant, was observed for the NSQs **3**, **4**, **6,** and **7**, with quantum yields ranging between 0.2 and 0.3. On the other hand, the dianion derived from NSQs **1**(X = H) showed a low quantum yield ($\Phi_f < 0.05$), while that from NSQ **2** (Nafth) and **5** (X = COMe) could not be evaluated due to the chemical degradation of the dianions.

3.3. Chemical stability of NSQs

The evident degradation of NSQ dianion **2**, and to a lesser extent **5**, raises the issue of the chemical stability of NSQs in the highly alkaline media used in these experiments. Fig. 4D shows the time-course of the fluorescence intensity band of NSQ dianions **3**–**8** measured at the fluorescence intensity maxima. For NSQs **1**, **2**, and **9**, which are weakly fluorescent and non-fluorescent, respectively, we measured the evolution of the absorption bands of their dianionic forms. We noticed three different situations, i) fluorescent and chemically stable; ii) non-fluorescent but chemically stable; and iii) fluorescent but unstable dianion. Fig. 4A shows the perfect match among consecutive emission spectra of NSQ **8** (X = CN), for example, recorded over 2 h. Remarkably, the emission spectra of dianion **8** remained unaltered even after 15 h in the alkaline medium used in this experiment (99:1 v/v DMSO-H_2O mixture, 0.1 N NaOH solution). Fig. 4B, corresponding to NSQ **9** (X = NO_2), exemplifies a non-fluorescent but chemically stable NSQ dianion. In general, the dianionic nature of the N-squaraine fluorophores protects from the nucleophilic attack by the hydroxide that leads to hydrolytic degradation. However, Fig. 4C, recorded from NSQ **2** (Napth) shows the fluorescence evolution of the worst-case among those already studied. Here, the fluorescence of the dianion rapidly diminishes until almost its complete disappearance after 2 h due to hydrolytic degradation to the squaramate anion and the concomitant formation of the corresponding 1-naphthylamine as demonstrated by NMR and fluorescence degradation experiments performed on NSQ **2** (see, Supplementary Data, Figs. S19 and S20).

One can safely argue that the pK_a of this compound is very high (>15.5). Therefore, the acid-base equilibrium would compete with the nucleophilic attack of the hydroxide on the iminium bond of the mono- or doubly protonated NSQ **2** (Scheme 3). However, it is worth mentioning that the acidity strength of NSQ **1** (X = H), akin to that of NSQ **2**, proved stable enough in the same alkaline media. Thus, some other factors, perhaps the extended aromatic system of the naphthyl moiety, could decrease the activation energy of the nucleophilic attack and, together with the low acidity of the NSQ **2** protons, could significantly speed its degradation process.

3.4. DFT calculations

Density functional theory (DFT) calculations of several NSQs were carried out to get further insight into the absorption and emission properties of NSQ dianions. The geometry optimization (B3LYP/def2-TZVP) and absorption/emission properties of the NSQs were computed using first-principles calculations and the path integral approach developed by de Sousa et al. [45] The calculated λ_{max} values, principal orbital transitions, and oscillator strength (*f*) values are presented in Table 3. The calculated λ_{max} values are in acceptable agreement with the experimental values with absolute errors ranging from 3.7% for **5**–15.2% for **3**. The larger error observed for compound **3** is likely related to its tetra-anionic nature and the possible existence of acid-base equilibria. For all the NSQs studied, the observed UV bands correspond to $S_0 \rightarrow S_1$ excitations attributed to the HOMO → LUMO transition that embraces the central $C_4O_2N_2$ ring and the two arenes. As shown in Fig. 5, this transition involves intramolecular charge transfer from the central $C_4O_2N_2$ anionic core to only two C-atoms of the four-membered ring (those not bonded to oxygen), similarly to previously reported studies on SQs [52,53]. Additionally, the HOMO → LUMO transitions shown in Fig. 5 entail $\pi \rightarrow \pi^*$ transitions in both aromatic rings, including the substituents. Compared to **1**, the substituents extend the conjugation of the system, thus increasing the λ_{max} values. The substituents also increase the spatial overlap of the HOMO and LUMO orbitals, thus favoring the HOMO → LUMO transition. For Compound **2**, where the HOMO → LUMO transition is 90%, two additional transitions (~5%) were observed, which are described in the SI (see Fig. S21).

The emission results of NSQs have also been analyzed theoretically to

provide further insight into the fluorescence observed in compounds **1**–**8**. For all NSQs, the $S_1 \rightarrow S_0$ emission corresponds to the transition of LUMO to HOMO. The predicted emission energies range from 457 nm for **1 to** 643 nm for **5**, which can be assigned to an intramolecular charge transfer transition, as common in conjugated molecules. In general, the excellent agreement between the predicted and observed emission gives reliability to the path integral approach. The largest difference (10% error) was obtained for NSQ **1**. The calculated fluorescence rates at 298 K for all the molecules tested are presented in Table 4, disclosing similar k_f values. These rate constants are very similar to those reported by Kubota et al. for a series of fluorescent bis(pyrrol-2-yl)squaraines [49] and suggest that the NSQs analyzed herein decay from the S_1 state to the S_0 state via the radiation transition channel by fluorescence emission. However, the fact that all compounds exhibit similar theoretical k_f values disagrees with the low quantum yields observed for compounds **1** and **4**, see Table 2. For these compounds a competitive non-radiative mechanism likely occurs.

4. Conclusion

In summary, we reported the microwave-assisted synthesis of symmetrical N-squaraines. These compounds are weakly acidic and can be deprotonated with hydroxide bases in DMSO-H_2O solvent mixtures. The resulting N-squaraine dianions feature a highly negative central squaryl core flanked by two *para*-substituted electron-deficient arenes. The ionized NSQs showed intense emission fluorescence with quantum yields ranging from 0.2 to 0.7. The absorption ($S_0 \rightarrow S_1$) and emission ($S_1 \rightarrow S_0$) transitions occur in the visible, depending on the substituent. Relevant to this study is the high resistance to chemical degradation of N-squaraine dianions, likely due to a protective effect caused by repulsion between the participating negative species. Given that N-squaraine fluorescence has been poorly studied so far, these compounds open a way to develop effective absorption and fluorescent probes based on N-squaraines derived from primary anilines.

CRediT authorship contribution statement

Manel Vega: Conceptualization, Methodology, Investigation. **Rosa M. Gomila:** Software. **Jordi Pons:** Investigation. **Antonio Frontera:** Software, Formal analysis, Writing – review & editing. **Carmen Rotger:** Conceptualization, Supervision. **Antonio Costa:** Conceptualization, Supervision, Writing – review & editing.

Declaration of competing interest

The authors declare that they have no known competing financial interests or personal relationships that could have appeared to influence the work reported in this paper.

Data availability

Data will be made available on request.

Acknowledgments

The authors acknowledge the "Ministerio de Ciencia e Innovación" of Spain (project PID2020-115637 GB-I00 Feder funds), and the Govern de les Illes Balears (AP_2021_010), for financial support.

Appendix A. Supplementary data

Supplementary data to this article can be found online at https://doi.org/10.1016/j.dyepig.2022.110746.

References

[1] Law KY. Organic photoconductive materials: recent trends and developments. Chem Rev 1993;93:449–86. https://doi.org/10.1021/cr00017a020.
[2] He J, Jo YJ, Sun X, Qiao W, Ok J, Kim T il, et al. Squaraine dyes for photovoltaic and biomedical applications. Adv Funct Mater 2021;31. https://doi.org/10.1002/ADFM.202008201.
[3] Gsänger M, Bialas D, Huang L, Stolte M, Würthner F. Organic semiconductors based on dyes and color pigments. Adv Math 2016;28:3615–45. https://doi.org/10.1002/adma.201505440.
[4] Chen G, Sasabe H, Igarashi T, Hong Z, Kido J. Squaraine dyes for organic photovoltaic cells. J Math Chem A 2015;3:14517–34. https://doi.org/10.1039/C5TA01879J.
[5] Xiao Q, Yang S, Wang R, Zhang Y, Zhang H, Zhou H, et al. Synthesis, structure and material properties of thiopyranylidene-based asymmetrical squaraines. Dyes Pigments 2018;154:137–44. https://doi.org/10.1016/J.DYEPIG.2018.03.003.
[6] Ros-Lis Jv, Martínez-Máñez R, Sancenón F, Soto J, Spieles M, Rurack K. Squaraines as reporter units: insights into their photophysics, protonation, and metal-ion coordination behaviour. Chem Eur J 2008;14:10101–14. https://doi.org/10.1002/CHEM.200800300.
[7] Grande V, Shen CA, Deiana M, Dudek M, Olesiak-Banska J, Matczyszyn K, et al. Selective parallel G-quadruplex recognition by a NIR-to-NIR two-photon squaraine. Chem Sci 2018;9:8375–81. https://doi.org/10.1039/C8SC02882F.
[8] Barbero N, Butnarasu C, Visentin S, Barolo C. Squaraine dyes: interaction with bovine serum albumin to investigate supramolecular adducts with aggregation-induced emission (AIE) properties. Chem Asian J 2019;14:896–903. https://doi.org/10.1002/asia.201900055.
[9] Chang HJ, Bondar Mv, Liu T, Liu X, Singh S, Belfield KD, et al. Electronic nature of neutral and charged two-photon absorbing squaraines for fluorescence bioimaging application. ACS Omega 2019. https://doi.org/10.1021/acsomega.9b00718.
[10] Karpenko IA, Collot M, Richert L, Valencia C, Villa P, Mély Y, et al. Fluorogenic squaraine dimers with polarity-sensitive folding as bright far-red probes for background-free bioimaging. J Am Chem Soc 2015;137:405–12. https://doi.org/10.1021/ja5111267.
[11] Zhai C, Schreiber CL, Padilla-Coley S, Oliver AG, Smith BD. Fluorescent self-threaded peptide probes for biological imaging. Angew Chem Int Ed 2020;59:23740–7. https://doi.org/10.1002/anie.202009599.
[12] Mayerhöffer U, Gsänger M, Stolte M, Fimmel B, Würthner F. Synthesis and molecular properties of acceptor-substituted squaraine dyes. Chem Eur J 2013;19:218–32. https://doi.org/10.1002/CHEM.201202783.
[13] Sreejith S, Carol P, Chithra P, Ajayaghosh A. Squaraine dyes: a mine of molecular materials. J Math Chem 2008;18:264–74. https://doi.org/10.1039/b707734c.
[14] Sreejith S, Divya KP, Ajayaghosh A. A near-infrared squaraine dye as a latent ratiometric fluorophore for the detection of aminothiol content in blood plasma. Angew Chem Int Ed 2008;47:7883–7. https://doi.org/10.1002/anie.200803194.
[15] Ohsedo Y, Miyamoto M, Tanaka A, Watanabe H. Synthesis and electrochemical properties of symmetric squarylium dyes containing diarylamine. Dyes Pigments 2014;101:261–9. https://doi.org/10.1016/j.dyepig.2013.09.047.
[16] Gauger J, Manecke G. Kondensationsprodukte der Quadratsäure mit primären und sekundären Aminen, I. Chem Ber 1970;103:2696–706. https://doi.org/10.1002/cber.19701030839.
[17] Balcerak A, Kwiatkowska D, Iwińska K, Kabatc J. Highly efficient UV-Vis light activated three-component photoinitiators composed of tris(trimethylsilyl)silane for polymerization of acrylates. Polym Chem 2020;11:5500–11. https://doi.org/10.1039/d0py00763c.
[18] Balcerak A, Iwińska K, Kabatc J. Dyes and Pigments spectroscopic studies. Dyes Pigments 2019;170:107596. https://doi.org/10.1016/j.dyepig.2019.107596.
[19] Xia G, Liu Y, Ye B, Sun J, Wang H. A squaraine-based colorimetric and F-dependent chemosensor for recyclable CO2 gas detection: highly sensitive off-on-off response. Chem Commun 2015;51:13802. https://doi.org/10.1039/c5cc04755b. –5.
[20] Ilina K, MacCuaig WM, Laramie M, Jeouty JN, McNally LR, Henary M. Squaraine dyes: molecular design for different applications and remaining challenges. Bioconjugate Chem 2020;31:194–213. https://doi.org/10.1021/acs.bioconjchem.9b00482.
[21] Ros-Lis Jv, García B, Jiménez D, Martínez-Máñez R, Sancenón F, Soto J, et al. Squaraines as fluoro-chromogenic probes for thiol-containing compounds and their application to the detection of biorelevant thiols. J Am Chem Soc 2004;126:4064–5. https://doi.org/10.1021/ja031987i.
[22] Ros-Lis J v, Martínez-Mañez R, Soto J. A selective chromogenic reagent for cyanide determination. Chem Commun 2002:2248–9.
[23] Bacher EP, Lepore AJ, Pena-Romero D, Smith BD, Ashfeld BL. Nucleophilic addition of phosphorus(iii) derivatives to squaraines: colorimetric detection of transition metal-mediated or thermal reversion. Chem Commun (J Chem Soc Sect D) 2019;55:3286–9. https://doi.org/10.1039/c9cc01243e.
[24] Johnson JR, Fu N, Arunkumar E, Leevy WM, Gammon ST, Piwnica-Worms D, et al. Squaraine rotaxanes: superior substitutes for Cy-5 in molecular probes for near-infrared fluorescence cell imaging. Angew Chem Int Ed 2007;46:5528–31. https://doi.org/10.1002/anie.200701491.
[25] Kabatc J, Kostrzewska K, Jurek K, Dobosz R, Orzeł Ł. 1,3-Bis(phenylamino) squaraine - photophysical and photochemical properties. Dyes Pigments 2016;127:179–86. https://doi.org/10.1016/j.dyepig.2015.12.027.
[26] Balcerak A, Iwińska K, Kabatc J. Novel 1,3-bis(p-substituted phenylamino) squaraine dyes. The synthesis and spectroscopic studies. Dyes Pigments 2019;170:107596. https://doi.org/10.1016/j.dyepig.2019.107596.

[27] Vega M, Blasco S, García-España E, Soberats B, Frontera A, Rotger C, et al. Dual role of silver in a fluorogenicN-squaraine probe based on Ag(i)-π interactions. Dalton Trans 2021;50:9367–71. https://doi.org/10.1039/d1dt01408k.
[28] Law KY. Squaraine chemistry. Effects of structural changes on the absorption and multiple fluorescence emission of bis[4-(dimethylamino)phenyl]squaraine and its derivatives. J Phys Chem 1987;91:5184–93. https://doi.org/10.1021/j100304a012.
[29] Polishchuk V, Kulinich A, Rusanov E, Shandura M. Highly fluorescent dianionic polymethines with a 1,3,2-dioxaborine core. J Org Chem 2021;86:5227–33. https://doi.org/10.1021/acs.joc.1c00138.
[30] Kabatc J, Kostrzewska K, Kozak M, Balcerak A. Visible light photoinitiating systems based on squaraine dye: kinetic, mechanistic and laser flash photolysis studies. RSC Adv 2016;6:103851–63. https://doi.org/10.1039/c6ra23060a.
[31] Jurek K, Kabatc J, Kostrzewska K. The synthesis and spectroscopic studies of new aniline-based squarylium dyes. Dyes Pigments 2016;133:273–9. https://doi.org/10.1016/j.dyepig.2016.05.027.
[32] Prabhakar C, Bhanuprakash K, Rao VJ, Balamuralikrishna M, Rao DN. Third order nonlinear optical properties of squaraine dyes having absorption below 500 nm: a combined experimental and theoretical investigation of closed shell oxyallyl derivatives. J Phys Chem C 2010;114:6077–89. https://doi.org/10.1021/jp908475n.
[33] Liu W, Wang H, Li Ch-J. Metal-free markovnikov-type Alkyne hydration under mild conditions. Org Lett 2016;18:2184–7. https://doi.org/10.1021/acs.orglett.6b00801.
[34] Wang Y, Li Y, Yan Q, Liu X, Xia G, Shao Q, et al. Benzocaine-incorporated smart 1,3-squaraine dyes: red emission, excellent stability and cell bioimaging. Dyes Pigments 2020;173:107977. https://doi.org/10.1016/j.dyepig.2019.107977.
[35] Cox RA, Stewart R. The ionization of feeble organic acids in DMSO-water mixtures. J Am Chem Soc 1976;98:488–94. https://doi.org/10.1021/ja00418a027.
[36] Golcu A, Tumer M, Demirelli H, Wheatley RA. Cd(II) and Cu(II) complexes of polydentate Schiff base ligands: synthesis, characterization, properties and biological activity. Inorg Chim Acta 2005;358:1785–97. https://doi.org/10.1016/j.ica.2004.11.026.
[37] El-Sherif AA, Shoukry MM, Abd-Elgawad MMA. Protonation equilibria of some selected α-amino acids in DMSO-water mixture and their Cu(II)-complexes. J Solut Chem 2013;42:412–27. https://doi.org/10.1007/s10953-013-9966-0.
[38] Neese F. Software update: the ORCA program system, version 4.0. WIREs Comput Molec Sci 2018;8. https://doi.org/10.1002/wcms.1327.
[39] Becke AD. Density-functional exchange-energy approximation with correct asymptotic behavior. Phys Rev A 1988;38:3098. https://doi.org/10.1103/PhysRevA.38.3098.
[40] Lee C, Yang W, Parr RG. Development of the Colle-Salvetti correlation-energy formula into a functional of the electron density. Phys Rev B 1988;37:785–9. https://doi.org/10.1103/PHYSREVB.37.785.
[41] Becke AD. Density-functional thermochemistry. III. The role of exact exchange. J Chem Phys 1993;98:5648–52. https://doi.org/10.1063/1.464913.
[42] Weigend F, Ahlrichs R. Balanced basis sets of split valence, triple zeta valence and quadruple zeta valence quality for H to Rn: design and assessment of accuracy. Phys Chem Chem Phys 2005;7:3297–305. https://doi.org/10.1039/b508541a.
[43] Petrenko T, Kossmann S, Neese F. Efficient time-dependent density functional theory approximations for hybrid density functionals: analytical gradients and parallelization. J Chem Phys 2011;134. https://doi.org/10.1063/1.3533441.
[44] Hirata S, Head-Gordon M. Time-dependent density functional theory within the Tamm–Dancoff approximation. Chem Phys Lett 1999;314:291. https://doi.org/10.1016/S0009-2614(99)01149-5.
[45] de Souza B, Neese F, Izsák R. On the theoretical prediction of fluorescence rates from first principles using the path integral approach. J Chem Phys 2018;148:034104. https://doi.org/10.1063/1.5010895.
[46] Park SY, Jun K, Oh SW. The novel functional chromophores based on squarylium dyes. Bull Kor Chem Soc 2005;26:428–32. https://doi.org/10.5012/bkcs.2005.26.3.428.
[47] Olmstead WN, Margolin Z, Bordwell FG. Acidities of water and simple alcohols in dimethyl sulfoxide solution. J Org Chem 1980;45:3295–9. https://doi.org/10.1021/JO01304A032/ASSET/JO01304A032.FP.PNG_V03.
[48] Schade A, Menzel R, Görls H, Spange S, Beckert R. Negative solvatochromism of an anionic thiazole-based dye. Asian J Org Chem 2013;2:498–503. https://doi.org/10.1002/ajoc.201300085.
[49] Gans P, Sabatini A, Vacca A. Investigation of equilibria in solution. Determination of equilibrium constants with the HYPERQUAD suite of programs. Talanta 1996;43:1739–53. https://doi.org/10.1016/0039-9140(96)01958-3.
[50] Hansch C, Leo A, Taft RW. A survey of Hammett substituent constants and resonance and field parameters. Chem Rev 1991;91:165–95. https://doi.org/10.1021/cr00002a004.
[51] Chen MC, Chen DG, Chou PT. Fluorescent chromophores containing the nitro group: relatively unexplored emissive properties. Chempluschem 2021;86:11–27. https://doi.org/10.1002/cplu.202000592.
[52] Kubota Y, Nakazawa M, Lee J, Naoi R, Tachikawa M, Inuzuka T, et al. Synthesis of near-infrared absorbing and fluorescent bis(pyrrol-2-yl)squaraines and their halochromic properties. Org Chem Front 2021;8:6226–43. https://doi.org/10.1039/D1QO01169C.
[53] Meyers F, Chen C-T, Marder SR, Brédas J-L, Meyers F. Electronic structure and linear and nonlinear optical properties of symmetrical and unsymmetrical squaraine dyes. Chem Eur J 1997;3:530–7. https://doi.org/10.1002/chem.19970030408.